

Sensorless Control of Direct-Current-Feed Doubly Fed Induction Generators Using T-Type Inverter

Hadi Afsharirad^{1*} | Fahimeh Sadighi-Amandi² | Mohamad Reza Banaei³ | Sara Misaghi⁴
 Department of Electrical Engineering, Azarbaijan Shahid Madani University, Tabriz, Iran. ^{1,2,3,4}
 Corresponding author's email: h.afsharirad@azaruniv.ac.ir

Article Info	ABSTRACT
<p>Article type: Research Article</p> <p>Article history: Received: 19-December-2024 Received in revised form: 09-March-2025 Accepted: 18-March-2025 Published online: 22-Dec-2025</p> <p>Keywords: DFIG-DC, FOC, Sensorless control, T-type inverter.</p>	<p>The use of DFIG-DC systems without stator voltage and current sensors has gained attention due to reduced costs and simplified control. However, diode rectifiers in these systems introduce current harmonics, degrading power quality and limiting performance at higher power levels. This study proposes a new structure for DFIG-DC systems, replacing the conventional two-level inverter with a T-type converter to address these issues. The proposed system uses a T-type converter to enhance voltage levels, reducing current harmonics and improving power quality. It also eliminates stator voltage and current sensors, simplifying the control system and reducing costs. Performance analysis through MATLAB/Simulink simulations demonstrated the effectiveness of the proposed system compared to conventional methods. The proposed DFIG-DC system with a T-type converter offers a cost-effective and efficient solution for reducing current harmonics and improving power quality. Its simplified control system and enhanced performance make it a promising approach for high-power applications in wind energy systems and other industrial uses. These findings highlight the system's potential for improving reliability and operational efficiency in renewable energy and industrial applications.</p>

NOMENCLATURE			
<i>DFIG</i>	Doubly-Fed Induction Generators	<i>MMF</i>	magnetomotive force
<i>MRF</i>	Multiple Reference Frame	<i>THD</i>	Total Harmonic Distortion
<i>NMCEC</i>	Normalized Maximum Corr-Entropy Criterion	<i>SOGI</i>	Second Order Generalized Integrator
<i>RSC</i>	Rotor Side Converter	<i>FLL</i>	Frequency Locked Loop

I. Introduction

The use of DC transmission systems has gained significant attention in recent years. These systems are widely utilized as transmission lines interconnecting power networks [1]. Furthermore, DC networks eliminate certain power electronic converters, simplifying the network structure and facilitating the integration of renewable energy sources and storage systems while offering high efficiency and flexibility in power distribution [2].

One of the key features of doubly-fed induction generator (DFIG) is their ability to independently control active and reactive power, enabling variable-speed AC power generation using only rotor-side converter control. This characteristic has made DFIGs widely adopted in wind

turbines [3]. The output power of a DFIG can be regulated by controlling the rotor currents. Consequently, the rotor side of the generator is connected to the DC network through a controlled converter, while the AC output from the stator is transferred to the same DC network via a diode bridge this structure, known as DFIG-DC. This approach reduces costs and simplifies the system [4, 5]. The main goals in this structures are to control the output power and the stator frequency, while DC link voltage regulation is managed through auxiliary control mechanisms [6]. Despite the numerous advantages of DFIG-DC systems, the presence of a diode rectifier introduces current harmonics in the stator windings. This results in distortions in the stator voltage and

flux waveforms, leading to increased torque ripple and reduced equipment lifespan [7].

Various studies have been conducted to mitigate these current harmonics and their adverse effects on DFIG systems. In reference [8] a new method for power angle control of DFIG-DC has been proposed. This method directly controls the output power without relying on current and voltage models. Additionally, an improved direct resonant controller is utilized in this study to reduce torque ripple and current harmonics. Reference [9] highlights that reducing current harmonics directly lowers torque ripple. It employs a resonant controller to minimize current harmonics, thereby reducing system losses. Resonant controllers have demonstrated excellent tracking capability for harmonic reference signals at a pre-designed resonant frequency. However, they are designed to target a specific harmonic frequency and do not account for frequency variations [10]. Moreover, resonant controllers have certain drawbacks, such as dependence on machine parameters, design complexity, and the requirement for positive and negative sequence control in unbalanced systems. Therefore, utilizing methods that not only reduce harmonics but also minimize computational burden in current and torque ripple calculations can significantly enhance the control system's performance [11,12].

Reference [10] proposes a method based on the multiple reference frame (MRF) approach to reduce torque ripple in DFIG-DC systems. It compensates for stator flux distortion caused by the diode rectifier by ensuring the rotor current tracks a pulsating reference signal. This method employs an estimator and regulator based on the MRF framework to accurately compute and track fundamental harmonics. The MRF-based controller provides a satisfactory dynamic response under unbalanced load conditions; however, its ability to eliminate harmonics is weak. Additionally, tuning this type of controller is challenging, involving complex mathematical computations and requiring a large amount of memory [13].

In Reference [14], a normalized maximum Corr-entropy criterion (NMCC) is utilized to reduce torque ripple and network power fluctuations in hybrid wind-solar systems. This approach eliminates the need for harmonic separation and compensates for distortions and voltage imbalances, resulting in distortion-free rotor currents and balanced, sinusoidal network currents. According to previous studies, this control method only reduces torque ripple; however, further research is needed to simultaneously improve stator current quality during unbalanced grid voltages [15].

One effective method for reducing harmonics is the use of multilevel converters. These converters help minimize the size of the output filter and reduce stress on switches, making them highly valuable in renewable energy systems [16].

Common types of multilevel inverters include T-type, diode-clamped, H-bridge, and flying capacitor inverters.

Among these, the T-type inverter stands out due to its reduced circuit components, the requirement for only a single DC link for all phases, and other advantages. These features make it a practical choice for medium- and high-power applications. The unique design of T-type inverters makes them particularly useful in electric vehicles [17, 18].

Additionally, T-type inverters are widely used in applications such as uninterruptible power supplies (UPS) for critical infrastructure like data centers and hospitals. Despite their benefits, these power sources face challenges such as high total harmonic distortion (THD) and noise, which can impact local power quality. Multilevel inverters can effectively address these issues [19]. T-type inverters also significantly enhance motor performance by reducing the harmonic content of the voltage applied to motor terminals. Furthermore, the high dv/dt generated in power electronics-based inverters is a known cause of motor failure. Multilevel inverters mitigate this issue by reducing dv/dt , thereby preventing motor damage [20].

Therefore, multilevel inverters, particularly the T-type, offer significant advantages in various industries, renewable energy systems, electric vehicles, and electric propulsion for aircraft. They are also widely used in energy storage systems, energy conversion management in microgrids, and smart grid applications.

In this study, the focus is on employing a three-level T-type converter within a DFIG-DC system to address key challenges in power quality and control. The proposed approach highlights the advantages of integrating a T-type inverter, which effectively reduces stator current and voltage harmonics. This reduction leads to lower torque ripple, output power ripple, and harmonic losses, thereby enhancing overall system performance. Unlike conventional methods, this work emphasizes the novel application of the T-type converter in a DFIG-DC context, demonstrating its potential to improve the control system's efficiency and reliability.

The control strategy, based on rotor current vectors, eliminates the need for stator current and voltage sensors, simplifying the system structure and reducing costs. Although sensorless control methods have been explored in previous studies, the innovative aspect of this research lies in the synergistic integration of the T-type converter with advanced control techniques. This integration results in a more precise, cost-effective, and robust system.

In comparison to existing approaches, reference [21] highlights the use of a sensorless control method that involves modeling the system using a transformer between the stator and rectifier, considering 5th and 7th order voltage harmonics. The proposed scheme utilizes field-oriented control to enhance system performance. While the addition of a transformer improves stator voltage quality, it also increases costs and can lead to higher impedance in the circuit, potentially affecting overall system efficiency. This

increase in impedance needs careful analysis during the design and implementation phases.

Further, in reference [22] the stator winding voltages are calculated using the Second Order Generalized Integrator (SOGI) method, which is then used in a Frequency Locked Loop (FLL). Although this approach reduces costs, the high precision required for setting parameters like natural frequency can lead to issues in voltage estimation, disrupting the performance of the FLL block. Reference [23] explores a method based on rotor current vectors, eliminating the need for stator voltage and current models. This approach reduces system costs by removing sensors but does not fully address the effects of harmonics, which can impact the accuracy and stability of the control system.

To evaluate the effectiveness of the novel T-type inverter configuration, MATLAB/Simulink simulations were conducted, and the results were compared with conventional methods. The findings show significant improvements in power quality and control dynamics, emphasizing the suitability of the T-type inverter for advanced DFIG-DC systems.

II. Methodology

A. System Structure of DFIG-DC

The overall schematic of the DFIG-DC system is illustrated in Fig. 1. In this configuration, the rotor side is connected to the DC network via a rotor side converter (RSC), while the stator side is connected to the same DC network through a diode-based rectifier.

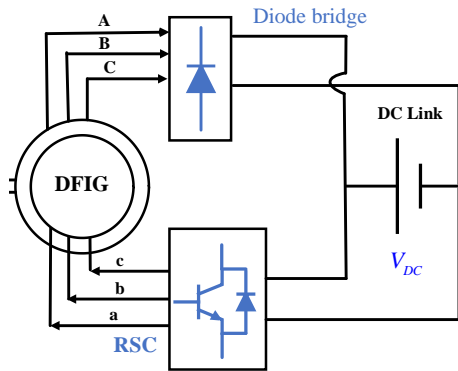


Fig. 1. Topology of a Conversion for a DFIG-DC System

The operational principle of a DFIG connected to a DC network involves two key processes: first, the excitation current is injected into the rotor windings via the RSC. Then, the power generated in the stator windings is transferred to the DC network through the stator-side rectifier.

In the DFIG system, the stator frequency is higher than the rotor frequency, and Fig.1 must be controlled in such a way that the MMF of the rotor windings is greater than that of the stator, as the control is performed from the rotor side. By

adjusting the MMF, the generated torque can be effectively controlled.

Fig. 2 illustrates the equivalent circuit of the DFIG in the stator flux-oriented frame. In this figure; I_r and I_s represent the rotor and stator currents, respectively. V_r and V_s denote the rotor and stator voltages. $L_{\sigma r}$, $L_{\sigma s}$ and L_m refer to the leakage inductance of rotor and stator and mutual inductance. R_r and R_s indicate the rotor and stator resistances. ψ_s and ψ_r correspond to the stator and rotor flux, respectively. ω_r represents the angular frequency of the rotor winding voltages and currents, while ω_s represents the angular frequency of the stator winding voltages and currents.

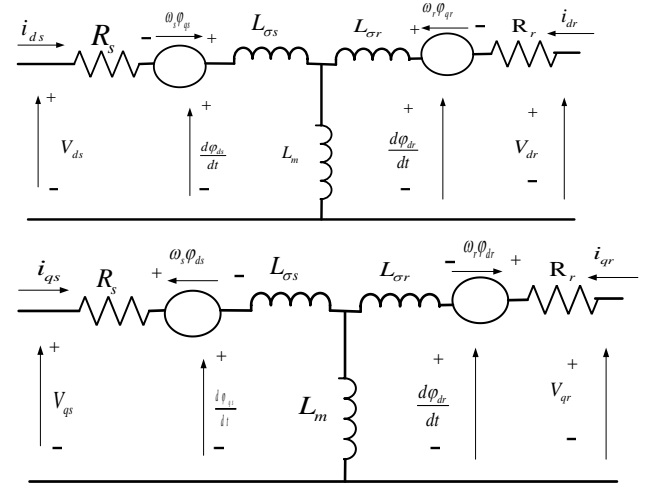


Fig. 2. Mathematical model of DFIG-DC

The stator and rotor voltage vector equations in the dq-axis, represented by Eq. 1 and Eq. 2, are derived from the equivalent circuit shown in Fig. 2. These equations can be expressed as follows:

$$\vec{V}_s = R_s \vec{i}_s + \frac{d\vec{\varphi}_s}{dt} + j\omega_s \vec{\varphi}_s \quad (1)$$

$$\vec{V}_r = R_r \vec{i}_r + \frac{d\vec{\varphi}_r}{dt} + j\omega_r \vec{\varphi}_r \quad (2)$$

The relationship between the flux and current vectors of the rotor and stator is expressed in Eq. 3 as follow.

$$\begin{cases} \vec{\varphi}_s = L_s \vec{i}_s + L_m \vec{i}_r \\ \vec{\varphi}_r = L_r \vec{i}_r + L_m \vec{i}_s \end{cases} \quad (3)$$

The torque equation can be defined using the stator flux and rotor current variables, as shown in Eq. 4.

$$T_{em} = \frac{3}{2} p \frac{L_m}{L_s} \text{Im} \left\{ \vec{\varphi}_s^* \vec{i}_r \right\} = \frac{3}{2} p \frac{L_m}{L_s} (\varphi_{sq} i_{rd} - \varphi_{sd} i_{rq}) \quad (4)$$

In this equation p represent as pole pair.

B. T-Type inverter

In the DFIG-DC system, one of the major challenges is the presence of voltage and current harmonics, which can disrupt the system's performance. These harmonics are primarily caused by the use of the diode rectifier, which introduces significant harmonic distortion.

One solution to reduce voltage and current harmonics is to use T-type inverters. In this approach, the focus is on rotor-side inverters. The T-type inverter has the ability to produce multiple voltage levels, which improves harmonic performance and facilitates the generation of high-quality output waveforms with a lower total harmonic distortion (THD).

In the T-type inverter, pulse width modulation effectively prevents direct switching between the positive (P) and negative (N) terminals.

The T-type converter structure is shown in Fig. 3. In this converter, nine switches are used, with three of them being bidirectional switches. The central point of the three-level inverter on the left is connected to the node "n". Additionally, the voltage across the bidirectional switches is half of the output voltage, which helps to reduce voltage stress and improve the overall performance of the inverter.

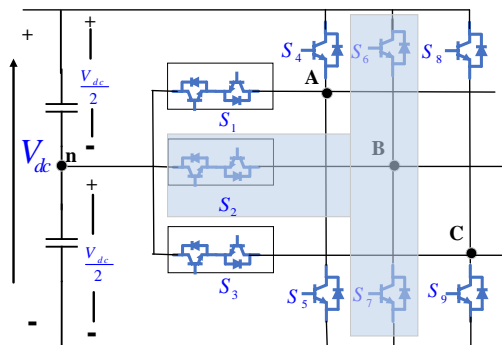


Fig. 3. Three phase three level T-Type inverter

Table 1 presents the switching states of the T-type converter for phase "A". To prevent a short circuit in the converter's DC link, the switches within a single leg must not be switched on at the same time. In this configuration, if switch S1 is turned on the phase "A" output voltage is set to zero. Activating switch S4 results in a phase "A" output voltage of $V_{dc}/2$, while turning on switch S5 sets the output voltage to $-V_{dc}/2$.

TABLE I SWITCHING MODES FOR PHASE A

Switching state	Phase voltage	S ₁	S ₄	S ₅
Case 1	0	On	Off	Off
Case 2	$V_{dc}/2$	Off	On	Off
Case 3	$-V_{dc}/2$	Off	Off	On

Table 2 provides an analysis of all voltage vectors and their corresponding switching states in the inverter. In the context of the three-phase system, there are 27 unique states, which are categorized into four main groups: zero states, small states, medium states, and large states.

TABLE 2 VOLTAGE VECTORS, SWITCHING STATES

State	On Switches	Voltage Vector
Zero vector	S_1, S_2, S_3	-
Zero vector	S_4, S_6, S_8	-
Zero vector	S_5, S_7, S_9	-
Small vector	S_1, S_7, S_9	\vec{V}_1
Small vector	S_4, S_2, S_3	\vec{V}_1
Small vector	S_4, S_6, S_3	\vec{V}_2
Small vector	S_1, S_2, S_9	\vec{V}_2
Small vector	S_1, S_6, S_3	\vec{V}_3
Small vector	S_5, S_2, S_9	\vec{V}_3
Small vector	S_1, S_6, S_8	\vec{V}_4
Small vector	S_5, S_2, S_3	\vec{V}_4
Small vector	S_1, S_2, S_8	\vec{V}_5
Small vector	S_5, S_7, S_3	\vec{V}_5
Small vector	S_4, S_2, S_8	\vec{V}_6
Small vector	S_1, S_7, S_3	\vec{V}_6
Medium vector	S_4, S_2, S_9	\vec{V}_7
Medium vector	S_1, S_6, S_9	\vec{V}_8
Medium vector	S_5, S_6, S_3	\vec{V}_9
Medium vector	S_5, S_2, S_8	\vec{V}_{10}
Medium vector	S_1, S_7, S_8	\vec{V}_{11}
Medium vector	S_4, S_7, S_3	\vec{V}_{12}
Large vector	S_4, S_7, S_9	\vec{V}_{13}
Large vector	S_4, S_6, S_9	\vec{V}_{14}
Large vector	S_5, S_6, S_9	\vec{V}_{15}
Large vector	S_5, S_6, S_8	\vec{V}_{16}
Large vector	S_5, S_7, S_8	\vec{V}_{17}
Large vector	S_4, S_7, S_8	\vec{V}_{18}

After excluding repetitive vectors, the T-type inverter features 21 unique independent vectors and it has 13 voltage vectors more than those in a conventional two-level inverter. This increase greatly reduces voltage harmonics, resulting in a corresponding decrease in current harmonics. The space vector diagram of the T-type inverter, shown in Fig. 4, is divided into 12 sectors. Each vector, excluding repetitive and zero vectors, corresponds to a specific switching state listed in Table 2.

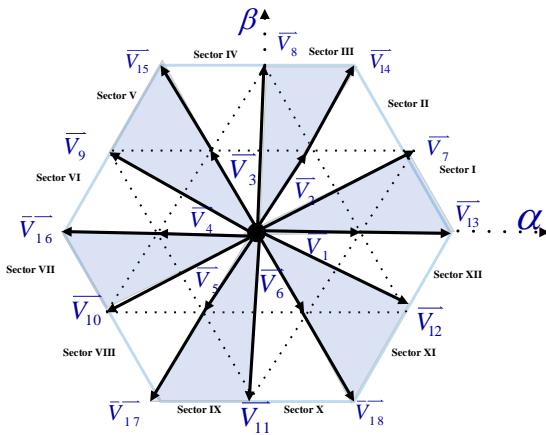


Fig. 4. T-Type inverter's voltage vectors' distribution in the $\alpha\beta$ plane

During diode rectifier conduction, the steady-state equivalent circuit of the DFIG connected to the diode bridge is illustrated in Fig. 5. For simplified analysis, the rotor variables are referenced to the stator side, with the RSC and rotor modeled as an equivalent current source, I_r . In this representation, I_m is the magnetizing current, I_s is the stator current, v_g denotes the air-gap voltage, and v_s represents the stator voltage.

Using the equivalent circuit depicted in Fig. 5, the relationship between the stator and rotor currents can be mathematically expressed as shown in Eqs. 5. This equation establishes the connection between the two current components, offering insight into their interdependence within the system's operational framework.

$$I_r = I_s + I_m \quad (5)$$

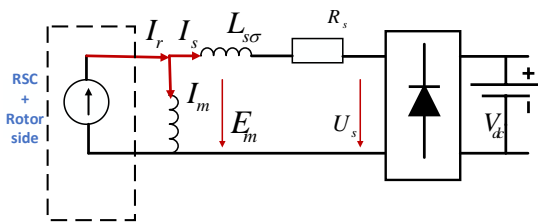


Fig. 5. Steady-State Equivalent Circuit of the DFIG-DC System

Given that the stator resistance is negligible compared to the stator leakage inductance, the air-gap voltage can be approximated and expressed as shown in Eq. 6.

$$E_m = j\omega_s L_m I_m = U_s + j\omega_s L_{s\sigma} I_s \quad (6)$$

Because the diode bridge causes the stator voltage to be nearly in phase with the stator current, the rotor current can be derived using Eqs. 5 and 6. The resulting expression is presented in Eq. 7.

$$I_r = -j \frac{U_s}{L_m \omega_s} + \frac{L_s}{L_m} I_s \quad (7)$$

In Eq. 7, L_s represents the sum of the mutual inductance and the stator leakage inductance. Using this equation, the

relationship between the stator current and the rotor current can be derived and expressed as shown in Eq. 8.

$$|I_r| \cos(\delta) = \frac{L_s}{L_m} |I_s| \rightarrow |I_s| = \frac{L_m}{L_s} |I_r| \cos(\delta) \quad (8)$$

The angle between the rotor current and the stator current is mathematically defined by Eq. 9. This equation captures the phase relationship between the two currents.

$$\delta = \arctan\left(\frac{|U_s|}{\omega_s L_s |I_s|}\right) \quad (9)$$

Using this angle, the stator power can be expressed as shown in Eq. 10. This equation incorporates the phase relationship between the rotor and stator currents to accurately represent the power dynamics in the system.

$$P_s = \frac{L_m}{L_s} |I_r| |U_s| \cos(\delta) \quad (10)$$

From Eq. 10, it is clear that the stator active power can be effectively controlled using rotor current vector control. When the stator power is reduced to zero, the stator current also becomes zero, aligning the stator voltage with the air-gap voltage. In this condition, the stator voltage is 90 degrees out of phase with the rotor current. As the power output increases, the stator current rises, causing a reduction in the phase angle. This phase angle remains constrained within the range of 0 to 90 degrees, ensuring stable operation and predictable power dynamics.

In DFIG-DC systems, control of the system relies entirely on the RSC because the diode rectifier on the stator side is uncontrollable. The RSC plays a dual role: it manages the power transferred from the rotor and ensures that the generator operates at its nominal frequency, thereby maintaining optimal performance. This makes the RSC a critical component in the system's overall functionality.

Sensorless controllers offer a promising solution to simplify the system by eliminating the need for stator voltage and current sensors. By reducing computational complexity, these controllers enhance system performance and enable more precise control over the stator side. In sensorless control, the system is managed using the rotor current vector, which effectively governs the dynamics of the generator without direct stator-side measurements.

The control scheme for the T-type converter, designed to regulate stator power and frequency, is depicted in Fig. 6. In this configuration, the DC voltage V_{dc} and DC current I_{dc} on the stator side are sampled along with the rotor currents and rotor position to manage the rotor-side converter.

This control scheme has two primary components: stator active power control and stator frequency control, both implemented through rotor current vector control. The stator frequency control block generates a slip angle, which is utilized for Park and Clarke transformations to transition between reference frames. Meanwhile, the active power control block ensures proper regulation of stator active

power by adjusting the rotor current vector, facilitating precise and stable operation of the DFIG-DC system.

In steady state, the stator frequency matches the rotational speed of the rotor current vector in the dq reference frame, which is directly determined by the rotor speed. By using the rotor angle and the synchronous dq frame angle, the slip angle can be calculated as shown in Eq. 11.

$$\theta_{slip} = \frac{1}{s} \omega_s - \theta_r \quad (11)$$

The stator power can be represented in terms of the DC voltage V_{dc} and DC current I_{dc} measured on the stator side, as expressed in Eq. 12.

$$P_s = V_{dc} I_{dc} \quad (12)$$

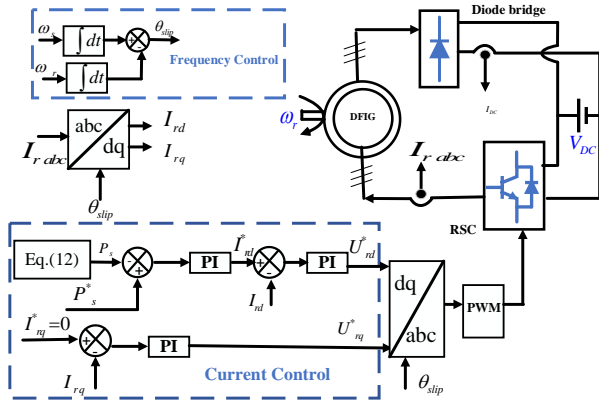


Fig. 6. Overall Control Scheme

The stator power is directly influenced by the rotor current, allowing it to be regulated through the magnitude of the rotor current. For maximum output power, the q-axis component of the rotor current should be controlled to zero, ensuring efficient power transfer. This relationship is formalized in Eq. 13, which outlines the method for controlling the stator active power via the rotor current.

$$I_{rd}^* = \frac{k_{pp}s + k_{ip}}{s} (P_s^* - P_s) \quad (13)$$

When the q-axis current is set to zero, the rotor current simplifies to equal the d-axis current. In this control framework, K_p represents the proportional gain, and K_i denotes the integral gain of the feedback controller.

The proportional and integral gains of the inner current control loop are selected based on the system's bandwidth requirements. The bandwidth of the outer power control loop is designed to be one-tenth of the inner loop's bandwidth. These choices ensure proper dynamic response and stability in both control loops.

Variations in controller parameters, such as K_p and K_i , can significantly impact the system's response, particularly in terms of harmonic content and overall system stability. The tuning of these parameters directly affects system damping and the magnitude of its response to external disturbances. Therefore, precise adjustment of these parameters is crucial

to achieving the desired power quality and control stability. For instance, in the rotor current control loop, the selection of K_p and K_i is made to achieve an appropriate open-loop bandwidth for rotor current, which is essential for maintaining system performance under varying operating conditions.

The controller design strategy aims to balance fast dynamic response and system stability. Specifically, the rotor current control loop is designed to respond faster than the power control loop, and its controller parameters are tuned to ensure that the open-loop transfer function achieves crossover at the desired frequency with an appropriate phase margin.

Using $K_p = 5.3$ and $K_i = 500$, the system's pole map has been plotted in fig.7. According to the transfer function of power loop shown in Eq.14 the results indicate that as the power varies from zero to one per-unit, the power control loop remains stable at all times [24].

$$\begin{aligned} \frac{\Delta P_s}{\Delta P_s^*} &= \frac{(sk_p + k_i) \frac{L_m u_s}{L_s} \cos \varepsilon_0}{s - (\sin^2 \varepsilon_0 - \frac{(sk_p + k_i) L_m u_s}{s L_s} \cos \varepsilon_0)} \\ &= \frac{(sk_p + k_i) \frac{L_m u_s}{L_s} / \cos \varepsilon_0}{s + \frac{(sk_p + k_i) L_m u_s}{L_s} / \cos \varepsilon_0} \end{aligned} \quad (14)$$

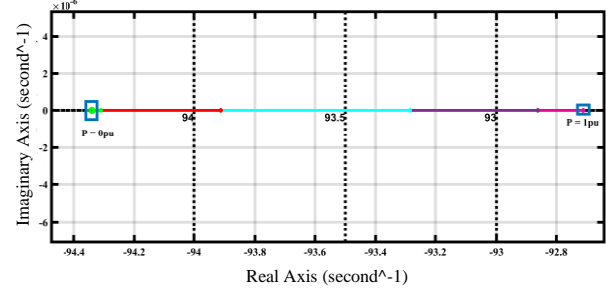


Fig. 7. Pole map of power control loop

III. TEST RESULTS

To assess the effectiveness of the proposed control strategy, simulations were conducted using the MATLAB/Simulink environment. The simulations were conducted on a system with an Intel Core i7 processor, 16 GB RAM, and MATLAB/Simulink R2021b. The average simulation time varied depending on the complexity of the model, with the proposed method requiring approximately 2% more computation time than conventional approaches due to the increased number of switching states and control calculations. However, the computational load remains manageable for real-time implementation with appropriate hardware.

The system's rotational speed is driven by a squirrel-cage induction motor mechanically coupled to the induction generator. The DC grid is modeled as a constant voltage source connected to a resistive load, simulating a realistic DC network. The specifications of the power supply and

squirrel cage induction motor match the specifications of the DFIG given in Table 3.

TABLE II Parameters of the DFIG

Parameters	Symbols	Value
Rated power	I_r	1000 W
Rated frequency	f_n	50 Hz
Rated voltage	V_n	110 V
Rotor resistance	R_r	0.88 Ω
Stator resistance	R_s	1.01 Ω
Mutual inductance	L_m	8.87 mH
DC voltage	V_{dc}	140 V
Stator leakage inductance	$L_{\sigma s}$	5.6 mH
Rotor leakage inductance	$L_{\sigma r}$	5.6 mH

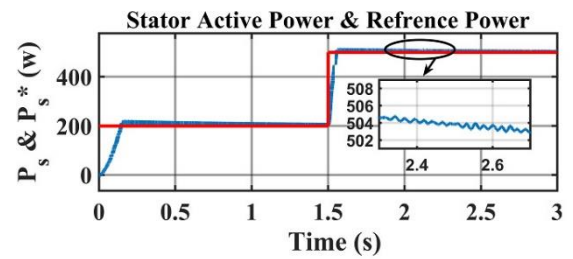
This setup provides a robust framework for analyzing the performance improvements achieved by the proposed control strategy.

Fig. 8 illustrates the system's behavior in two stages. In the first stage, from $t=0$ s to $t=1.5$ s, a reference power of 200 is set, and the active power of the stator closely follows this reference value in both methods.

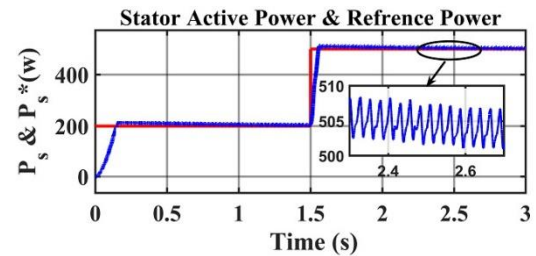
At $t=1.5$ t, the reference power is increased to 500. During this second stage, the active power of the stator reaches the desired value within 250 milliseconds without any steady-state error, as shown in Fig. 8(a). The proposed method achieves this with minimal fluctuations, and, compared to the conventional method shown in Fig. 8(b), the power ripple is significantly reduced.

Fig.9 shows the phase-to-phase rotor voltage. As can be seen, the output voltage of the T-type inverter has 5 levels, while the output voltage of the two-level inverter has 3 levels. The voltage range is the same for both methods. If the voltage levels are increased, the voltage harmonics are reduced because the waveform becomes closer to a sinusoidal shape due to the larger number of smaller voltage steps. Since the rotor voltage is positively correlated with the rotor current, the rotor current is also closer to an ideal sinusoid and the harmonics are reduced, and according to equation 8, the stator current is also improved, thereby reducing the harmonics of the entire system.

Reducing the harmonics of the rotor current directly affects the electromagnetic torque and reduces it, resulting in an overall improvement in the system. In addition, increasing the number of voltage levels increases the regulation of the MMF in the rotor, which is very important for maintaining optimal performance and controlling the power flow in the stator and rotor windings. Therefore, higher voltage levels contribute to a more stable system with less harmonic distortion.

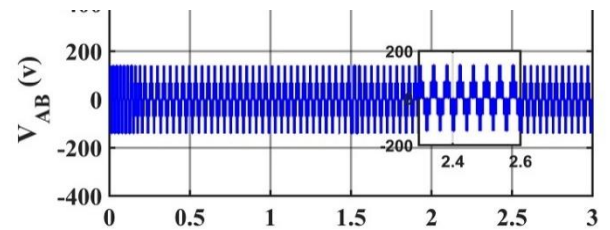


(a)

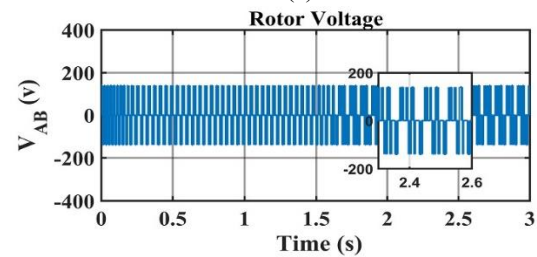


(b)

Fig. 8. The waveform of the stator active power and reference power. (a) Proposed Method (b) Conventional Method.



(a)



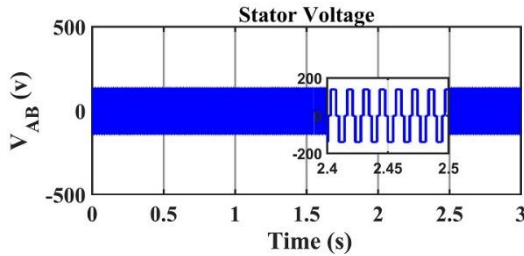
(b)

Fig. 9. Rotor Voltage Waveform (a) Proposed Method (b) Conventional Method

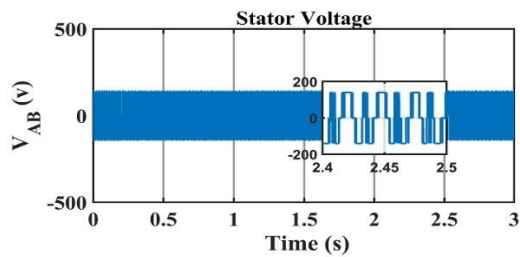
Fig. 10 shows the phase-to-phase stator voltage of the DFIG. As seen, the voltage amplitude is the same in both methods, but the voltage waveform in the proposed method is not only more desirable but also significantly has fewer harmonics compared to the conventional method. This reduction in harmonics contributes to improved power quality and optimized system performance.

Fig. 11 shows the torque behavior in both transient and steady-state conditions for both methods. A transient state occurs when the reference power changes from 200 to 500 at $t=1.5$ s. The figure clearly demonstrates that the proposed method leads to reduced torque ripple in the steady-state, with the torque value reaching 1 N.m. In contrast, the

conventional method results in a steady-state torque value of 10 N.m.

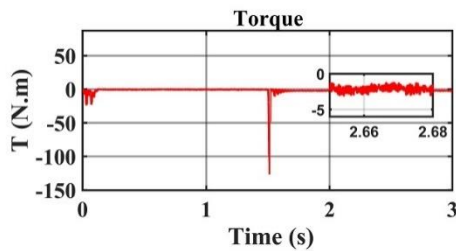


(a)

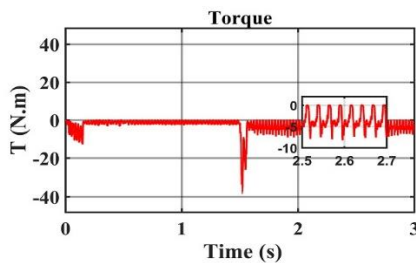


(b)

Fig. 10. Stator Voltage Waveform (a) Proposed Method (b) Conventional Method



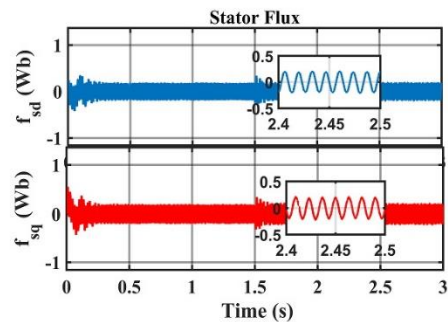
(a)



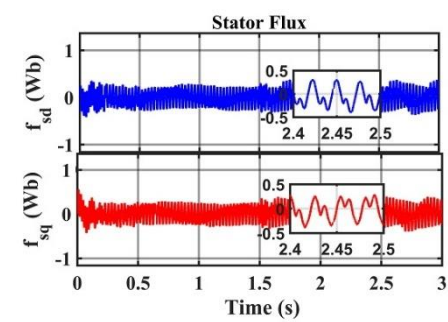
(b)

Fig. 11. Torque Waveform. (a) Proposed Method (b) Conventional Method

Fig. 12 and 13 illustrate the flux waveforms of the stator and rotor in the dq reference frame. The results from $t = 2.4$ s to $t = 2.5$ s indicate that the proposed method significantly reduces harmonics, leading to flux components in this reference frame exhibiting fewer variations and approaching nearly constant values. This demonstrates the optimal performance of the proposed control method in improving flux quality, highlighting its capability to reduce fluctuations and enhance system stability.

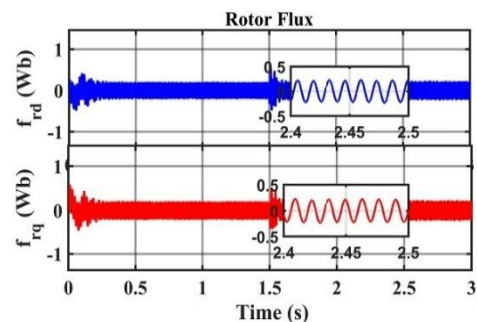


(a)

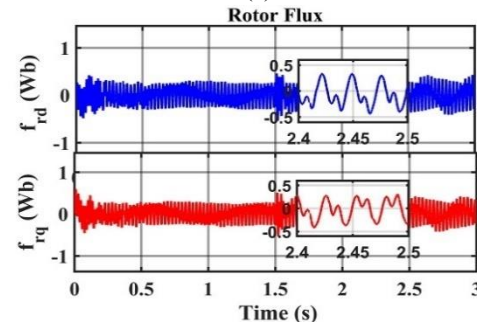


(b)

Fig. 12. Stator Flux Waveform (a) Proposed Method (b) Conventional Method



(a)



(b)

Fig. 13. Rotor Flux Waveform (a) Proposed Method (b) Conventional Method

The response to the step change in reference power for the stator and rotor currents for both control methods is shown in Fig. 14 and 15, respectively. By comparing the steady-state changes in Fig. 14 from $t = 2.45$ s to $t = 2.49$ s, it is observed that the proposed method significantly reduces the harmonics of the stator currents, and the waveform is much

closer to an ideal sine wave. Similarly, this comparison in the steady-state for the rotor current waveforms is clearly evident in Fig. 15. The results indicate that by using the T-type inverter, three-phase currents for both the rotor and stator can be achieved with better quality.

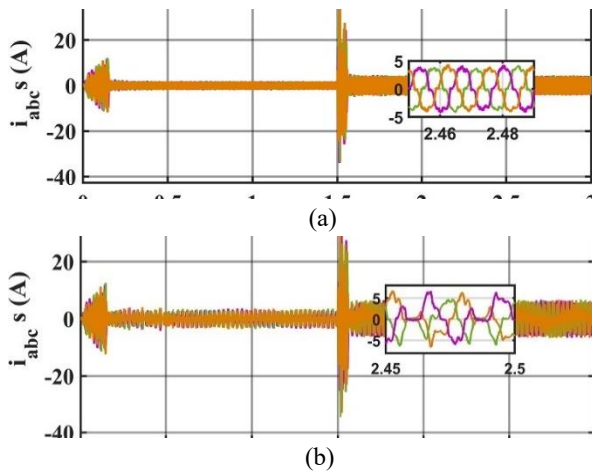


Fig. 14. Stator Current Waveform (a) Proposed Method (b) Conventional Method

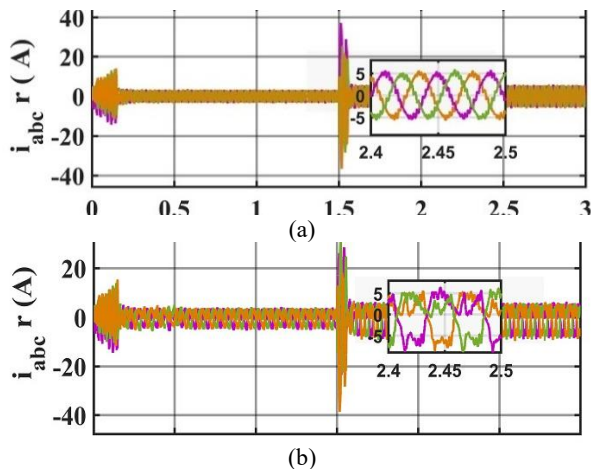


Fig. 15. Rotor Current Waveform (a) Proposed Method (b) Conventional Method

These results demonstrate the effectiveness of the proposed method in improving power quality and reducing harmonics. Fig. 16 shows the FFT analysis of rotor current harmonics in the steady-state, where the harmonic content for the conventional method is 52.26%, and for the proposed method, it is 13.09%. Additionally, Fig. 17 illustrates the FFT analysis of stator current harmonics in the steady-state, which is 51.76% for the conventional method and 14.43% for the proposed method.

Reducing harmonics can significantly enhance system performance, and the T-type inverter plays a crucial role in achieving this by offering advantages such as reduced distortion and improved sinusoidal voltage generation with fewer components. However, despite these benefits, the T-type inverter also introduces certain challenges. Compared

to a conventional two-level inverter, it requires a more complex circuit topology due to the increased number of switches, making the switching process more challenging. Nonetheless, its ability to minimize harmonics and improve overall efficiency makes it a valuable choice in power electronics applications.

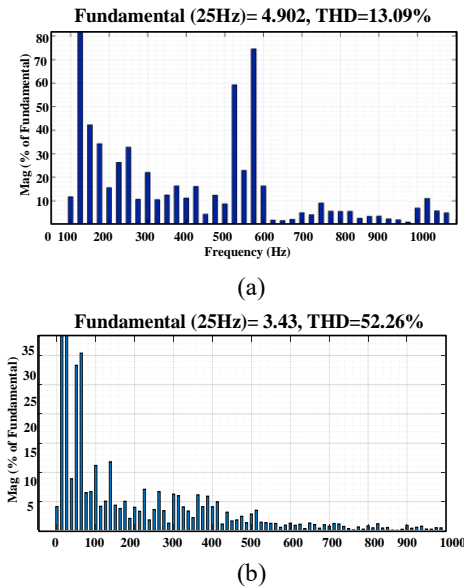


Fig. 16. FFT Analysis of Rotor Current (a) Proposed Method (b) Conventional Method

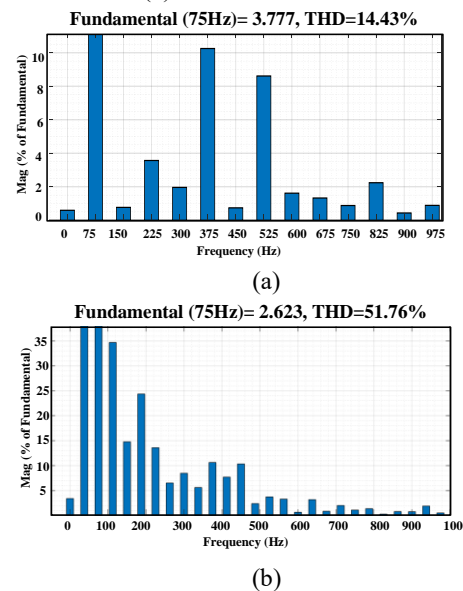


Fig. 17. FFT Analysis of Stator Current (a) Proposed Method (b) Conventional Method

IV. Conclusion

In this study, a novel approach for controlling a DFIG-DC system has been introduced through the integration of a three-level T-type inverter, leading to significant improvements in power quality and control performance.

Unlike conventional methods, which primarily focus on mitigating characteristic harmonics of the form $6n \pm 1$, the

proposed approach has been designed to effectively reduce lower-order harmonics such as the 5th and 7th without requiring additional complex control strategies. This improvement has been achieved while maintaining a relatively simple control structure, minimizing mathematical complexity, and ensuring practical feasibility.

A key advantage of the proposed method is the elimination of stator voltage and current sensors, which has simplified the control system, reduced costs, and enhanced system reliability. Instead, a current-oriented control strategy has been employed to regulate stator frequency and DFIG-DC power. Although a slight increase in complexity on the power system side has been observed, a substantial reduction in current harmonics, torque ripple, and power ripple has been demonstrated, resulting in superior output performance.

Compared to the closest existing methods, which often rely on resonant or advanced controllers for harmonic suppression, better harmonic reduction has been achieved by utilizing the advanced capabilities of the T-type inverter while maintaining a more straightforward control framework. The effectiveness of this method has been validated through MATLAB/Simulink simulations, where improved dynamic response and harmonic suppression have been observed in comparison to traditional two-level inverters.

These findings provide new insights into improving power quality in DFIG-DC systems, and it is expected that the proposed method will serve as a viable and implementable solution for wind energy applications. By setting a new benchmark in renewable energy systems, this work is anticipated to contribute to future research on optimizing multi-level inverter-based control strategies for grid-connected and stand-alone wind power systems.

References

- [1] S. M. A. Cruz, G. D. Marques, P. F. C. Gonçalves and M. F. Iacchetti, "Predictive Torque and Rotor Flux Control of a DFIG-DC System for Torque Ripple Compensation and Loss Minimization," in *IEEE Transactions on Industrial Electronics*, vol. 65, no. 12, pp. 9301-9310, Dec. 2018, doi: 10.1109/TIE.2018.2818667.
- [2] R. Zhang et al., "Protection and Power Smoothing of a DFIG/DC Microgrid Hybrid Power System With SMES-Based Unified Power Quality Conditioner," in *IEEE Transactions on Applied Superconductivity*, vol. 34, no. 8, pp. 1-5, Nov. 2024, Art no. 5401005, doi: 10.1109/TASC.2024.3425322.
- [3] G. D. Marques and M. F. Iacchetti, "Minimization of Torque Ripple in the DFIG-DC System Via Predictive Delay Compensation," in *IEEE Transactions on Industrial Electronics*, vol. 65, no. 1, pp. 103-113, Jan. 2018, doi: 10.1109/TIE.2017.2716860.
- [4] C. Wu, P. Cheng, H. Nian and F. Blaabjerg, "Rotor Current Oriented Control Method of DFIG-DC System Without Stator Side Sensors," in *IEEE Transactions on Industrial Electronics*, vol. 67, no. 11, pp. 9958-9962, Nov. 2020, doi: 10.1109/TIE.2019.2956415.
- [5] A. Verma and A. K. Jain, "A Dual-VSI DFIG-Dc Voltage Generation System Based on Series Connected Dc-Link," in *IEEE Transactions on Industrial Electronics*, vol. 71, no. 11, pp. 13670-13681, Nov. 2024, doi: 10.1109/TIE.2024.3363760.
- [6] C. Wu, D. Zhou and F. Blaabjerg, "Direct Power Magnitude Control of DFIG-DC System Without Orientation Control," in *IEEE Transactions on Industrial Electronics*, vol. 68, no. 2, pp. 1365-1373, Feb. 2021, doi: 10.1109/TIE.2020.2970666.
- [7] C. Wu and H. Nian, "Sinusoidal Current Operation of a DFIG-DC System Without Stator Voltage Sensors," in *IEEE Transactions on Industrial Electronics*, vol. 65, no. 8, pp. 6250-6258, Aug. 2018, doi: 10.1109/TIE.2017.2786259.
- [8] C. Wu, D. Zhou, P. Cheng and F. Blaabjerg, "A Novel Power-Angle Control Method of DFIG-DC System Based on Regulating Air Gap Flux Vector," in *IEEE Transactions on Power Electronics*, vol. 36, no. 1, pp. 513-521, Jan. 2021, doi: 10.1109/TPEL.2020.3001967.
- [9] C. Wu and H. Nian, "Improved Direct Resonant Control for Suppressing Torque Ripple and Reducing Harmonic Current Losses of DFIG-DC System," in *IEEE Transactions on Power Electronics*, vol. 34, no. 9, pp. 8739-8748, Sept. 2019, doi: 10.1109/TPEL.2018.2888599.
- [10] Y. Xiao, B. Fahimi, M. A. Rotea and Y. Li, "Multiple Reference Frame-Based Torque Ripple Reduction in DFIG-DC System," in *IEEE Transactions on Power Electronics*, vol. 35, no. 5, pp. 4971-4983, May 2020, doi: 10.1109/TPEL.2019.2941957.
- [11] X. Wang, D. Sun and Z. Q. Zhu, "Resonant-Based Backstepping Direct Power Control Strategy for DFIG Under Both Balanced and Unbalanced Grid Conditions," in *IEEE Transactions on Industry Applications*, vol. 53, no. 5, pp. 4821-4830, Sept.-Oct. 2017, doi: 10.1109/TIA.2017.2700280.
- [12] G. D. Marques and M. F. Iacchetti, "DFIG Topologies for DC Networks: A Review on Control and Design Features," in *IEEE Transactions on Power Electronics*, vol. 34, no. 2, pp. 1299-1316, Feb. 2019, doi: 10.1109/TPEL.2018.2829546.
- [13] S. Bhattacharyya, S. Puchalapalli and B. Singh, "Operation of Grid-Connected PV-Battery-Wind Driven DFIG Based System," in *IEEE Transactions on Industry Applications*, vol. 58, no. 5, pp. 6448-6458, Sept.-Oct. 2022, doi: 10.1109/TIA.2022.3181124.
- [14] S. Das and B. Singh, "Normalized Maximum Correntropy Criterion Based Ripple Mitigation Strategy for Wind-Solar Hybrid Generation System Under Nonideal Grid Conditions," in *IEEE Transactions on Power Electronics*, vol. 38, no. 1, pp. 956-967, Jan. 2023, doi: 10.1109/TPEL.2022.3199387.
- [15] S. Das and B. Singh, "Islanding Operation and Seamless Resynchronization in DFIG-SPV System Equipped With Functional Enhancements Through ATLLAD Control Framework," in *IEEE Transactions on Power Electronics*, vol. 38, no. 6, pp. 7634-7643, June 2023, doi: 10.1109/TPEL.2023.3259443.
- [16] M. Lak, B. -R. Chuang and T. -L. Lee, "A Common-Mode Voltage Elimination Method With Active Neutral Point Voltage Balancing Control for Three-Level T-Type Inverter," in *IEEE Transactions on Industry Applications*, vol. 58, no. 6, pp. 7499-7514, Nov.-Dec. 2022, doi: 10.1109/TIA.2022.3201175.
- [17] A. Sheir, M. Z. Youssef and M. Orabi, "A Novel Bidirectional T-Type Multilevel Inverter for Electric Vehicle Applications," in *IEEE Transactions on Power*

Electronics, vol. 34, no. 7, pp. 6648-6658, July 2019, doi: 10.1109/TPEL.2018.2871624.

- [18] Kenneth E. Okedu, "Augmenting DFIG wind turbine transient performance using alternative voltage source T-type grid side converter," *Renewable Energy Focus*, vol.18,2017,Pages 1-10,ISSN 1755-0084,https://doi.org/10.1016/j.ref.2017.02.004.
- [19] Sánchez Vargas, Oscar, Luis Gerardo Vela Valdés, Monica Borunda, Ricardo Eliú Lozoya-Ponce, Jesus Aguayo Alquicira, and Susana Estefany De León Aldaco. 2024. "ANFIS-PSO-Based Optimization for THD Reduction in Cascaded Multilevel Inverter UPS Systems" *Electronics* 13, no. 22: 4456.
- [20] Y. El. Khelifi, A. El. Magri, A. Mansouri, R. Lajouad, "Enhanced low voltage ride-through control of multilevel flying capacitor inverter based wind generation," *Indonesian Journal of Electrical Engineering and Computer Science*, vol.33,no.6, pp.: 854-861, Feb. 2024. DOI:10.11591/ijeecs.v33.i2.pp854-861.
- [21] H. Misra and A. K. Jain, "Analysis of Stand-Alone DFIG-DC System and DC Voltage Regulation With Reduced Sensors," in *IEEE Transactions on Industrial Electronics*, vol. 64, no. 6, pp. 4402-4412, June 2017, doi: 10.1109/TIE.2017.
- [22] C. Wu, H. Nian, B. Pang and P. Cheng, "Adaptive Repetitive Control of DFIG-DC System Considering Stator Frequency Variation," in *IEEE Transactions on Power Electronics*, vol. 34, no. 4, pp. 3302-3312, Apr. 2019, doi: 10.1109/TPEL.2018.2854261.
- [23] C. Wu, Y. Jiao, H. Nian and F. Blaabjerg, "A Simplified Stator Frequency and Power Control Method of DFIG-DC System Without Stator Voltage and Current Sensors," in *IEEE Transactions on Power Electronics*, vol. 35, no. 6, pp. 5562-5566, June 2020, doi: 10.1109/TPEL.2019.2953677.
- [24] D.Zhou, F. Blaabjerg., "Bandwidth oriented proportional-integral controller design for back-to-back power converters in DFIG wind turbine system," *IET Renewable Generation*, Vol.11, no.7, pp. 941-951, June. 2017, doi:org/10.1049/iet-rpg.2016.0760.



Hadi Afsharirad was born in Abhar, Iran, in 1985. He received the B.Sc. degree from the Zanzan University, Iran and M.Sc. and Ph.D. degrees, from the University of Tabriz, Tabriz, Iran, in 2008, 2010, and 2018, respectively, all in electrical engineering. He is an Assistant Professor with the Department of Electrical Engineering, Azarbaijan Shahid Madani University, Tabriz, which he joined in 2020. His main research interests include the electric and hybrid electric vehicles, renewable energy, linear electric machines and electrical drives.



Fahimeh Sadighi-Amandi was born in Tabriz, Iran, in 1997. she received the B.Sc degree from the Payame Noor University of Tabriz and M.Sc degree from the Azarbaijan Shahid Madani University, Tabriz, Iran in 2021, 2024 respectively. Her main research interests include electric machines, renewable energy and electrical drives.



Mohamad Reza Banaei was born in Tabriz, Iran. He received the M.Sc. degree in control engineering from the Polytechnic University of Tehran, Tehran, Iran, in 1999, and the Ph.D. degree in power engineering from the Faculty of Electrical Engineering, Tabriz University, Tabriz, in 2005. He is currently a Professor with the Department of Electrical Engineering, Azarbaijan Shahid Madani University, Tabriz, where he joined in 2005. His main research interests include the designing and controlling of power electronic converters, renewable energy systems, modeling and controlling of FACTS and custom power devices, and power systems dynamics.



Sara Misaghi was born in Iran, in 1997. she received the B.Sc. & M.Sc. degree from the Azarbaijan Shahid Madani University, Tabriz, Iran in 2018, 2024. she is a Phd. student of Azarbaijan Shahid Madani University. Her main research interests include electric machines and electrical drives.